Materials Science & Engineering A 847 (2022) 143339

Contents lists available at ScienceDirect

Materials Science & Engineering A

journal homepage: www.elsevier.com/locate/msea

Influence of initial quenching on the microstructure and mechanical properties of quenched and partitioned ferritic stainless steels

Lassi Raami *, Pasi Peura

Materials Science and Environmental Engineering, Tampere University, P.O. Box 589, FI, 33014, Finland

ARTICLE INFO

Keywords:
Q&P
Ferritic stainless steels
Retained austenite

ABSTRACT

Modern steel industry has great interest in developing new advanced high-strength steels, especially for the automotive industry. The need for stronger and more ductile sheet steels has led to development of novel heat treatments such as quenching and partitioning. The Q&P heat treatment provides an opportunity of manufacturing strong steels without sacrificing their formability. However, there is limited research conducted on the microstructure evolution of many alloys potential for Q&P such as stainless steels.

This study evaluates the selection for the optimal quench interruption temperature during Q&P of ferritic stainless steels. The paper compares different simulation models for optimizing the Q&P-process. Q&P was applied to two AISI 420-type stainless steels EN 1.4021 and EN 1.4034 to assess the simulation results. Microstructure analyses with X-ray diffraction and electron microscopy revealed that simulated values overestimate the retained austenite fractions after Q&P due to formation of Cr-rich carbides. Mechanical tests showed that Q&P is applicable to grade EN 1.4021 stainless steel, whereas EN 1.4034 fractured in a brittle manner under tensile load. Electron microscopy revealed intergranular fracture type and concentration of Cr-rich carbides at parent austenite grain boundaries in EN 1.4034. These results suggest that impurities may expose stainless steels to temper embrittlement during partition.

1. Introduction

Modern steel industry is actively developing new advanced high-strength steels, known as AHSS, which have several applications amongst the technical fields. One of the target industries is the automotive industry, as stronger steel grades can offer significant improvements in the fuel economy and safety of automobiles. This has drawn attention to developing stronger sheet steel materials which could replace the conventional grades [1]. However, increasing the strength of steel may lead to deterioration of other properties. Traditionally, the strength and ductility of steel have been considered mutually exclusive. In conventional steel grades, increasing the strength generally results in reduction of ductility and vice versa. Therefore, to increase the formability without significant reduction of strength, novel third generation AHSS grades are being developed. These steels usually have complex microstructures which consist of a high-strength constituent, such as fine-grained martensite, combined with a ductile constituent such as austenite [2].

Quenching and Partitioning (Q&P) heat treatment, originally proposed by Speer et al. [3], is one possible method for producing such microstructure. The process begins with a full austenitization or intercritical annealing step, followed by initial quenching where the martensitic transformation is interrupted at an optimal quenching temperature (*QT*) between the martensite start (M_s) and finish temperatures (M_f). The steel is then held at a partition temperature (*PT*) usually greater than the *QT* and quenched to room temperature [3,4]. The aim of the partition stage is to stabilize the retained austenite remaining within the microstructure after the initial quench by carbon partitioning from martensite to austenite at *PT*. As these temperatures can vary in the range of 70–450 °C [5,6], competing mechanisms have to be suppressed with suitable alloying elements inhibiting the formation of carbides such as silicon or aluminium. Although the majority of Q&P studies have focused on low-alloyed Si or Al-containing steels [1], the process is also applicable to some high-alloy steels such as stainless steels [7–12]. Results from earlier studies [8,11] suggest that Q&P-processed stainless steels may reach ultimate tensile strength of up to 2000 MPa while maintaining decent (>10%) elongation. However, the Q&P process used for stainless steels is often simplified by initially quenching the steel to room temperature [8,10,11] instead of determining an optimal *QT*.

* Corresponding author.
E-mail address: lassi.raami@tuni.fi (L. Raami).

https://doi.org/10.1016/j.msea.2022.143339
Received 28 February 2022; Received in revised form 18 May 2022; Accepted 19 May 2022
Available online 22 May 2022

Hence, more research on the effect of initial quenching is needed.

The goal of Q&P heat treatment is to form a microstructure consisting of carbon-enriched austenite within a martensite matrix. In order to estimate the fraction of retained austenite, a thermodynamic methodology has been developed for determining the optimal quenching temperature [3,13,14]. This methodology relies on a model predicting martensitic transformation curve as a function of temperature as well as calculations of M_s temperature as a function of steel composition. The optimal QT is defined as the QT resulting in the maximum retained austenite fraction after the heat treatment. The selection of a proper QT is essential: setting the QT too high may result in unstable retained austenite, which may transform into secondary martensite during the final quenching. In contrast, setting the QT too low results in a small fraction of very stable retained austenite which might not transform to martensite during deformation. As a result, a suitable QT can only be within a narrow temperature range.

The methodology introduced by Speer et al. [3] proposes a model describing the lowest temperature for carbon partitioning between the phases during the heat treatment. This model relies on a condition, where the phase boundary is assumed to be stationary and the chemical potential of carbon is uniform in both phases, known as constrained para-equilibrium (CPE). This condition was later revised as constrained carbon equilibrium (CCE), as the term "constrained para-equilibrium" could be argued to be misleading due to the condition not being para-equilibrium by nature [15,16]. Under the CCE condition there is an infinite set of carbon concentrations that would result in uniform chemical potential of carbon within the phases. Thus, the initial austenite fraction and carbon content are first calculated as a function of quenching temperature, after which austenite carbon concentration changes during the partitioning. The most common equation used for determining the martensite phase fraction during quenching is the Koistinen-Marburger (K-M) equation [17]:

$$V_{\alpha'} = 1 - e^{[-K\times(M_s - T)]} \tag{1}$$

where $V_{\alpha'}$ is the volume fraction of primary martensite, K is an empirically chosen constant 0.011 and temperature T can be replaced with the initial quenching temperature QT. If the quenching is performed after full austenitization and other phase transformations are suppressed, the remaining phase is austenite. Although the original methodology has been extensively used for the selection of the initial quench temperature, it might not be suitable for all steels. Hence, this equation has been modified to consider the effect of alloying elements in several studies such as [18–20]. These modified equations, however, are usually applicable to only a narrow range of alloys. Furthermore, according to the authors' knowledge, no specific models have been developed for stainless steels, giving preference to the use of equation (1) in this study.

Another crucial step in the modelling of Q&P heat treatment is the determination of the M_s temperature. Over the years, several models [21–25] for determining the M_s temperature have been developed. Since the selection of model for the M_s calculation has a significant effect on the optimal QT, the used model must be selected specifically to a given composition, especially when the steel has high alloying contents. As this study focuses on stainless steels, the models should be selected from ones that can be applied to steels with high chromium content. The first model used is one proposed by Capdevila et al. [24]:

$$M_S(^\circ C) = 491.05 - 302.6C - 30.6Mn - 16.6Ni - 8.9Cr + 2.4Mo - 11.3Cu + 8.58Co + 7.4W - 14.5Si \tag{2}$$

This model is widely applicable as it was developed using artificial neural network based on hundreds of alloys over a wide range of alloying elements [24,26]. The equation (2) can be applied to steels containing 0–17.9 wt.-% of chromium [24]. Another model used in this study was developed by Finkler and Schirra [25]:

$$M_S(^\circ C) = 635 - 474[C + 0.86(N - 0.15(Nb + Zr)) - 0.066(Ta + Hf)] - (33Mn + 17Ni + 17Cr + 21Mo + 39V + 1W) \tag{3}$$

Equation (3) was developed for steels containing 8–14% of chromium [25], and it is therefore suitable for various stainless steel grades. In addition to empirical equations, the M_s temperature can also be determined with the CALPHAD (CALculation of PHAse Diagrams) approach using a simulation software such as JMatPro®. Although the JMatPro®-software does not contain direct calculation functions for simulating Q&P, it can be utilized by applying several M_s temperature calculations in a systematic manner. First, the M_s temperature of the alloy is calculated for full austenitization. The initial austenite carbon concentration is then presumed to correspond to the steel composition. For the partitioning step, it is presumed that the substitutional elements cannot migrate, and that interface migration of only carbon atoms is possible [3,27]. The M_s temperature is then simulated as a function of the austenite carbon concentration by repeating the calculation with differing carbon concentrations. The resulting correspondence can then be described as an equation of M_s temperature as a function of austenite carbon content which can be used for the simulated alloy similarly to any other equation.

The aim of this paper is to evaluate the optimal QT selection methodology for ferritic stainless steels during the Q&P heat treatment. Different M_s calculation models are used for predicting the optimal QT for two AISI 420-type stainless steels EN 1.4021 and EN 1.4034. These predictions are then assessed by comparison with experimental results: Q&P heat treatment with varying QT is applied to the examined steels. The resulting microstructure and retained austenite fraction are then investigated with X-ray diffraction and electron microscopy techniques. Furthermore, the microstructure evolution and its correspondence to the calculated models is discussed. Finally, the effect of QT on the mechanical properties is assessed with tensile tests followed by analysis of the fracture surfaces.

2. Experimental procedure

The steels used in this study were AISI 420-type ferritic stainless steel grades EN 1.4021, named further in the paper as steel A, and EN 1.4034, named as steel B, with chemical compositions shown in Table 1. The steels were delivered as cold rolled sheets with dimensions 2.0 mm × 1250.0 mm x 2500.0 mm for the steel A, and 6.0 mm × 1250.0 mm x 2000.0 mm for the steel B. Samples for the heat treatments were cut in plate thickness in a rectangular shape with rounded corners with width and height of 20.0 mm × 20.0 mm. The full austenitization temperatures were calculated using the JMatPro®-software (Fig. 1 a) & b)), and they were estimated as 980 °C for the steel A and 1100 °C for the steel B.

A schematic illustration of the used Q&P heat treatment is shown in Fig. 2. The samples from steel A were austenitized at 1020 °C for 5 min. The samples from steel B were austenitized at 1100 °C for 15 min: Due to the limitations of the used equipment, higher temperatures were not achieved and, hence, the austenitization time was extended to 15 min. However, as simulations in Fig. 1 b) indicated that all $M_{23}C_6$-type carbides should dissolve at 1050 °C, the temperature was presumed sufficient. All samples were quenched in oil for 10 s. The initial quenching temperatures were chosen based on the range of simulated values: 85 °C, 100 °C, 115 °C, 130 °C, 145 °C, 160 °C, and 170 °C. The required quenching rate to prevent carbide formation during cooling was

Table 1
Chemical compositions of examined steels (in wt.-%).

Steel grade	Code	C	Cr	Mn	Si	P	S	Fe
EN 1.4021	A	0.20	13.27	0.65	0.45	0.021	0.001	Bal.
EN 1.4034	B	0.45	13.7	0.55	0.35	0.029	0.002	Bal.

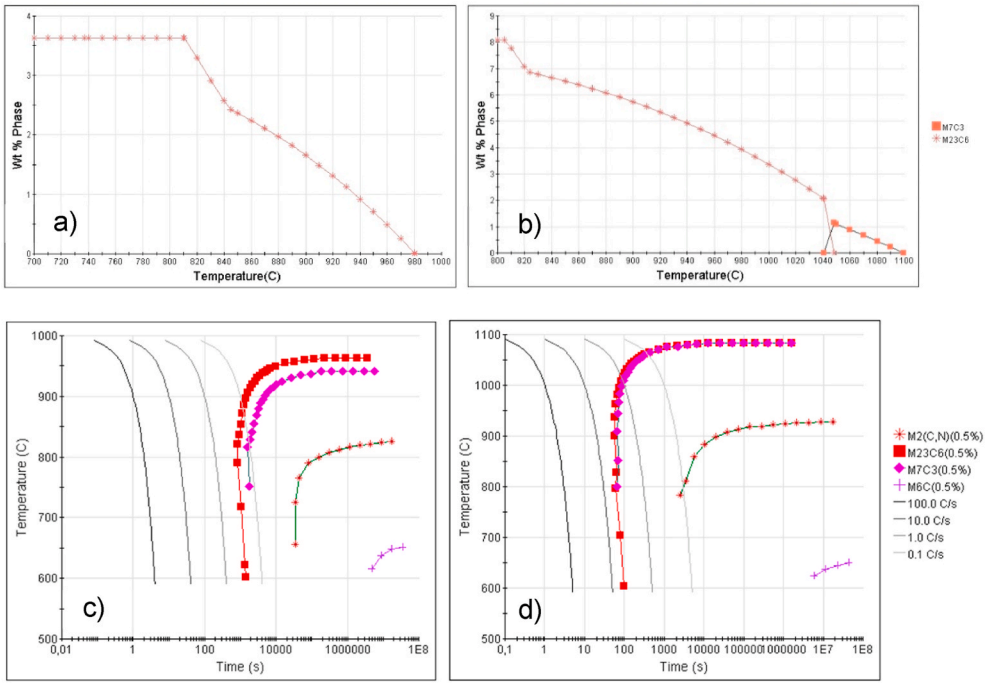

Fig. 1. Simulations for austenitization conditions with JMatPro®: Carbide phase fractions at austenitization temperature range a) for steel A and b) for steel B, and CCT from full austenitization for c) steel A and d) steel B.

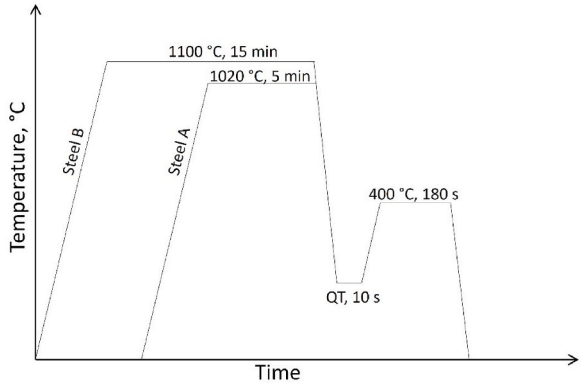

Fig. 2. Schematic diagram of the Q&P heat treatment. Quenching temperature QT varies from 85 °C to 170 °C for different samples. Final quenching was performed to room temperature.

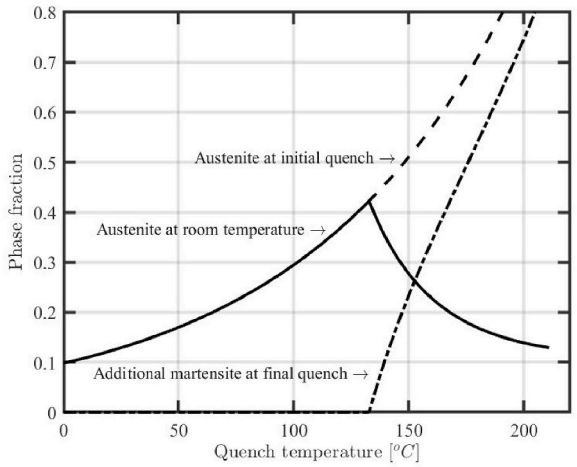

Fig. 3. Principle of the calculation of retained austenite fraction after Q&P.

estimated to be higher than 20 K/s based on simulations with JMatPro® as shown in Fig. 1 c) and d), as well as work by de Andrés et al. [28]. Quenching was immediately followed by partitioning treatment at 400 °C for 180 s. The partitioning temperature was chosen based on earlier work by Yuan et al. [8]. For reference purposes, two samples of each grade were quenched without partitioning treatment: one directly water-quenched from austenitization temperatures to room temperature and the other with initial quenching in oil at 130 °C for 10 s followed by water quenching. The purpose of the latter quenching was to allow slower cooling during quenching to avoid cracking of the samples.

The retained austenite phase fraction as a function of the initial quench temperature was calculated using a specific MATLAB script. Visual representation of the calculation is shown in Fig. 3. The calculation process consists of two steps. First, the austenite fraction after the initial quench is determined using the K-M equation. When the initial quenching temperature QT is increased, the austenite volume fraction increases, whereas the carbon content of the formed austenite decreases. Then, full carbon partition to austenite is assumed during the partitioning step. During this second calculation step the stability of the retained austenite is assessed by calculating its M_s temperature as a function of carbon content: As the carbon content of the austenite increases during the partition, the M_s temperature of the austenite is decreased. If the M_s temperature is not decreased below room temperature, secondary martensite will form upon the final quench. Hence, the phase fraction of retained austenite is reduced drastically. As a result, the highest volume fraction of retained austenite is obtained at the peak QT_{max}. Increasing the QT above this point will result in formation of brittle secondary martensite, which may deteriorate the mechanical properties of the steel. Thus, temperatures below QT_{max} should be preferred. This type of calculation was conducted for both steels with varying M_s calculation models based on Capdevila et al. [24], Finkler & Schirra [25], and JMatPro®.

The microstructural characterization was conducted using field emission scanning electron microscopy (FE-SEM), electron backscatter diffraction (EBSD) and energy-dispersive X-ray spectroscopy (EDS). The

volume fraction of austenite was measured with X-ray diffraction (XRD) and a combination of EBSD and EDS.

The FE-SEM system used was a Zeiss ULTRAplus field emission scanning electron microscope equipped with Oxford Instruments X-MaxN 80 energy dispersive X-ray spectroscope (EDS) and Oxford instruments Symmetry® CMOS EBSD detector. Samples for SEM observations were cold-mounted and prepared by standard mechanical grinding and polishing using Struers Tegramin-30 up to abrasive size of 1 μm, followed by etching with heated V2A etchant. The samples were then cleaned in ethanol in an ultrasonic cleaner and coated with a thin carbon layer using JEOL JEC-530 auto carbon coater. Samples for the EBSD analyses were prepared by mechanical grinding and polishing up to abrasive size of 0.02 μm with MasterMet 2 suspension. The sample surfaces were first cleaned with an ultrasonic cleaner in ethanol followed by finishing with an Emitech K1050X plasma cleaner.

XRD measurements were carried out using a Stresstech Xstress 3000 G2 X-ray diffractometer equipped with a Cr tube. The measurements were performed using CrK_{α}-radiation with a collimator size of 3 mm following the ASTM standard E957 – 13 [29]. The used voltage and current values were set at 30 kV and 6.7 mA. The detectors were equipped with filters to remove K_{β}-radiation. The measured 2θ-peaks were at 156.4° and 106.1° with an exposure time of 10 s for ferrite and at 130° and 79° with an exposure time of 30 s for austenite. These peaks correspond to diffraction lines h, k, l (211) and (200) for ferrite and (220) and (200) for austenite, respectively. Austenite peak (111) and ferrite peak (110) were excluded due to partial overlapping with each other. The measured data was analysed using XTronic 1.12.0 -software. Retained austenite fractions were first measured from raw data, followed by another calculation with correction factors according to the measured carbide fractions as described in standard [29].

Hardness tests were performed using Struers Duramin-A300 hardness testing system. The measurements were carried out as low-force Vickers hardness tests with a load of 2 kg (HV2) according to standard DIN EN ISO 6507. Tensile tests were performed for samples initially quenched at selected temperatures using Instron 8801 servohydraulic test system. The used initial quenching temperatures were 115 °C, 145 °C, and 170 °C for the steel A and 100 °C, 130 °C, and 160 °C for the steel B, respectively. Sample dimensions were set at 2 mm × 4 mm with a gauge length of 20 mm for the steel A and 4 mm × 5 mm with a gauge length of 30 mm for the steel B. The strain rate was set to 1 x 10^{-3} s^{-1}. The strain was measured with LaVision StrainMaster digital image correlation system using 5-megapixel camera resolution. Additionally, the fracture surfaces of the samples were studied with SEM, and hardness tests were performed to the deformed samples. Finally, the retained austenite fractions of the deformed samples were measured with XRD.

3. Results

The microstructures of the investigated steels are shown in Fig. 4 for the steel A and Fig. 5 for the steel B. The as-received structure of the steels (Fig. 4 a) & Fig. 5 a)) contains ferrite covered with chromium carbide particles. After quenching (Fig. 4 b) & Fig. 5 b)), the microstructures comprise martensite with a small fraction of chromium carbides visible as light particles. Severe cracking visible to naked eye was observed in samples directly quenched to room temperature and, hence, they were excluded from the study. After the Q&P heat treatment the microstructures consist of martensitic matrix with small amounts of carbides (Fig. 4 c) & Fig. 5 c)). A slight increase in the carbide content can be seen, as the initial quenching temperature is increased (Fig. 4 d) & Fig. 5 d)). Rough surface structure can be seen in some samples (Fig. 5 c)), which may be due to over-etching resulting from the used hot-acid etching method. The contrast in SEM signal was set to reveal Cr-rich particles as light areas, after which the acquired image was processed with the ImageJ software. An example of the resulting polarized image is shown in Fig. 6.

The measured carbide fractions after the heat treatments are presented in Fig. 7. Before the heat treatment in as-received (A-R) condition the steels contain roughly ten percent carbides, which are then dissolved during the austenitization. However, as the directly quenched (DQ) samples contain a small fraction of carbides, the solution of carbides was

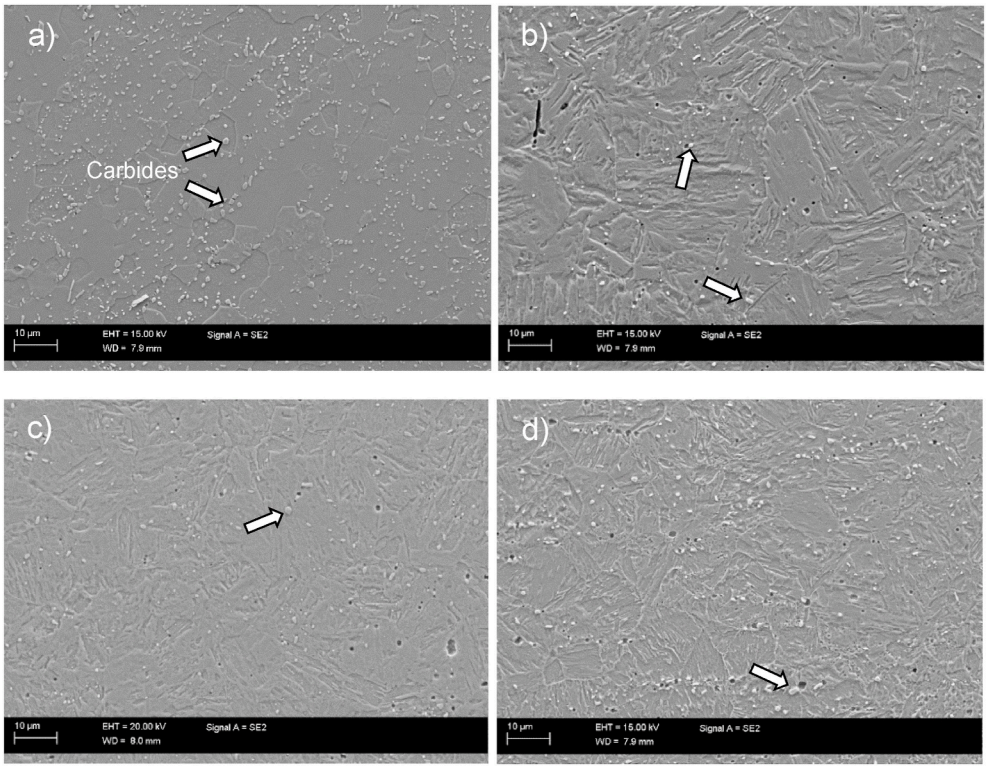

Fig. 4. SEM micrographs of the steel A: a) As-received condition, b) after quenching, and after Q&P with c) QT 115 °C and d) QT 160 °C.

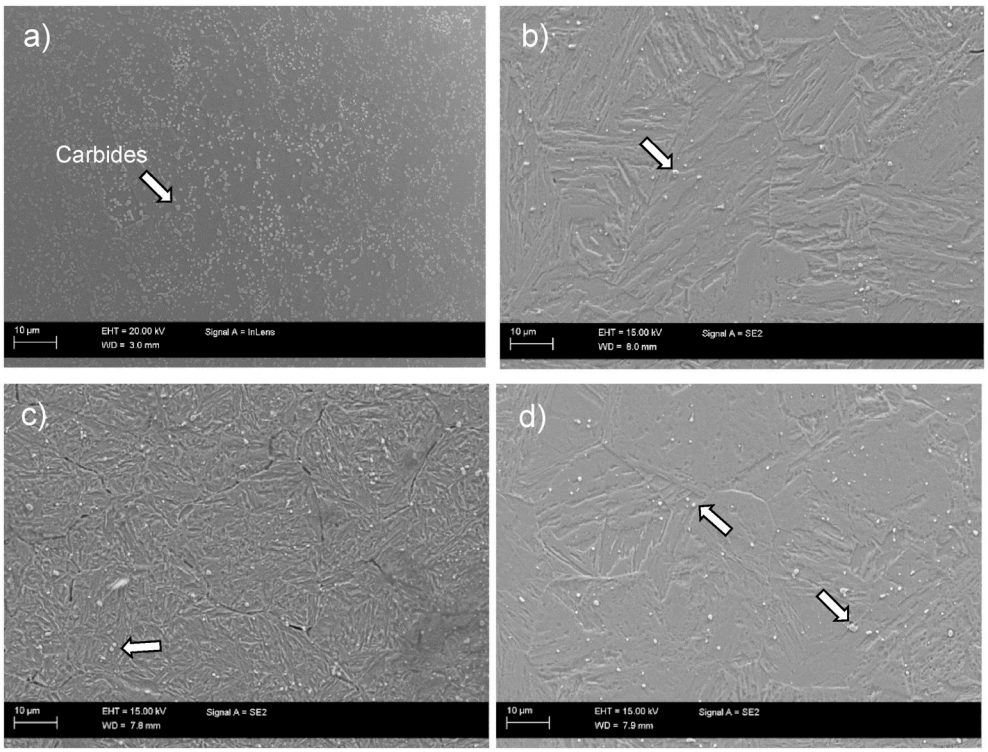

Fig. 5. SEM micrographs of the steel B: a) As-received condition, b) after quenching, and after Q&P with c) QT 100 °C and d) QT 160 °C.

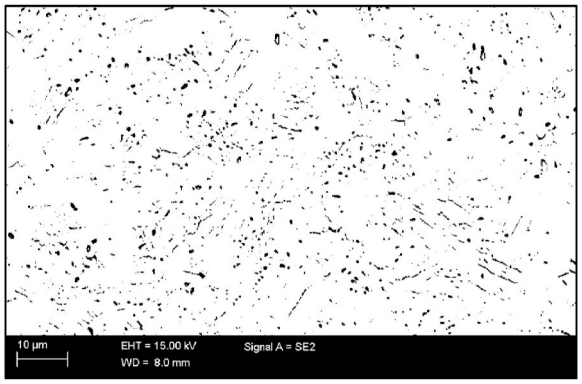

Fig. 6. Example of carbide distribution after contrast polarization with ImageJ, taken from steel A after Q&P with QT 145 °C.

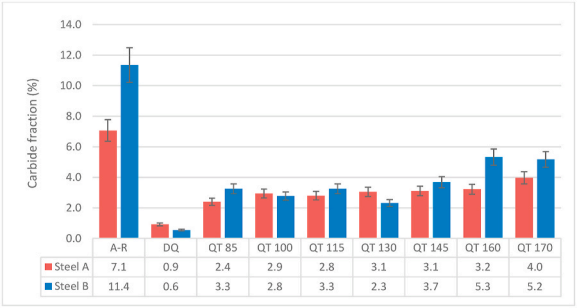

Fig. 7. Measured carbide fractions in as-received condition (A–R), after quenching without partition (directly quenched, DQ), and after Q&P heat treatments.

not fully complete at the end of the austenitization. After the Q&P heat treatment the samples contain up to five percent carbides, with the carbide content increasing as the initial quenching temperature is raised.

The EBSD micrographs of the steels are shown in Figs. 8 and 9 for steels A and B, respectively. The used acceleration voltage was 12 kV in all micrographs, with a step size of 0.060 µm and working distance varying between 8.5 and 9 mm depending on sample geometry and examined area. Samples which were not partitioned contain traces of retained austenite. The microstructure of the steels comprises rough martensitic structure with the original austenite grain boundaries visible as thick, non-indexed lines. It is also possible to observe some round particles, which the EDS detector identified as chromium-rich carbides. All EBSD images contain small fraction of carbides, which could be seen in the EDS-spectra in Fig. 10. These carbides were identified as chromium carbides, as they can be observed in Fig. 10 as chromium- and carbon-rich, iron-depleted areas. However, carbides were excluded from the EBSD phase list, as the observed crystal symmetries of certain carbide types can be nearly identical to the martensite phase. Hence, two adjacent datapoints near a carbide particle could be identified as different phases despite having very similar diffraction patterns, and the exact phase cannot be resolved by the software. After the Q&P heat treatment the EBSD patterns show that the martensitic laths within the grains have been refined compared to the quenched samples. This results from tempering of martensite during partition. Additionally, blocks of retained austenite are observed between the martensite laths. In the steel A, increasing the initial *QT* seems to increase the retained austenite fraction slightly, although the visible fraction is small compared to the simulated values. It is possible that some of the retained austenite data is lost in the black regions, where no EBSD patterns could be resolved. In the steel B, the highest austenite fraction was detected in the sample initially quenched at 100 °C. The microstructure consists of fine blocks of retained austenite in-between martensite laths. Although the patterns contain relatively high proportion of non-indexed data, the parent grains can be outlined from the orientation of Euler angles. Additionally, some round carbide particles can be identified. At a higher quenching

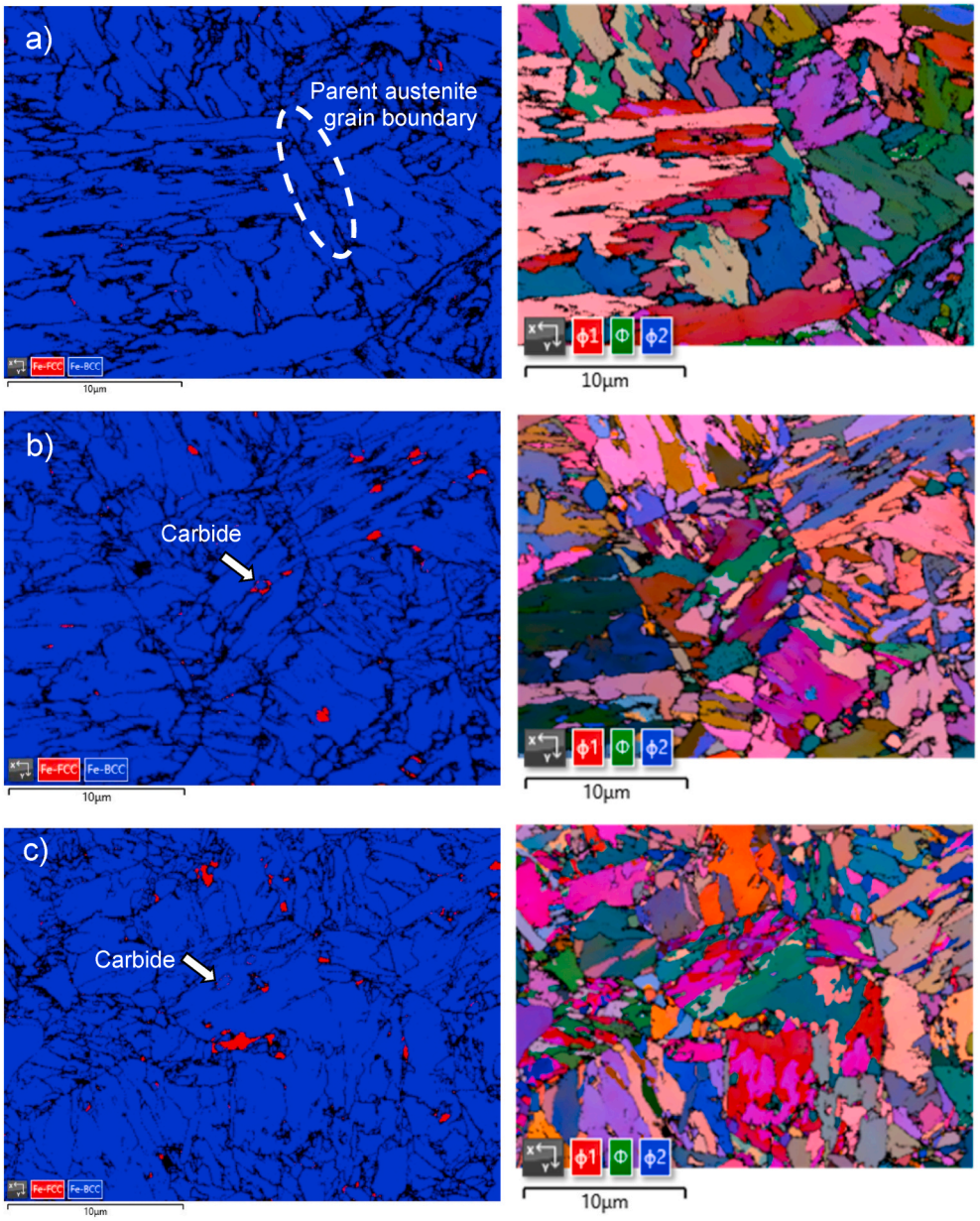

Fig. 8. EBSD micrographs of the phase distribution and Euler angles of the steel A: a) As quenched, and after Q&P with QT of b) 115 °C, and c) 170 °C.

temperature of 160 °C, practically no retained austenite can be resolved, and the structure comprises finely dispersed martensitic laths as well as a small number of round carbide particles. The near absence of retained austenite and high fraction of non-indexed data indicate that the used *QT* was too high, and the retained austenite was transformed into secondary martensite upon the final quenching to room temperature.

The retained austenite fractions were first calculated from the raw XRD-data. However, as the possible presence of carbides affects the obtained data, new calculations were made while considering the carbide fractions from Fig. 7. The results of both retained austenite (RA) fraction measurements are listed in Table 2 as a function of initial quenching temperature *QT*. Additionally, samples which had only undergone a quenching treatment were analysed for reference. After the quenching step, the samples had insignificant amounts of retained austenite. For the steel A the RA fraction seems to increase as the *QT* is raised. For the steel B a highest retained austenite fraction is achieved at *QT* of 100 °C, after which the RA fraction decreases as the *QT* is further increased.

Fig. 11 shows the simulated estimates for retained austenite fractions in comparison with the measured data. The measured values show relatively high variance due to the used measurement method. As several types of chromium carbides may interfere with the (220)-peak of austenite [29], the background noise for that peak is higher than for others. Therefore, the measured peak intensity appears lower, resulting in higher error estimation. Intensity calculation using only austenite peak (200) gives higher estimates for retained austenite fraction for all samples. When comparing the simulated values, all M_s temperature models seem to give higher fractions of retained austenite than what was measured. The equation (3) proposed by Finkler and Schirra [25] seems to provide closest estimate for the optimal quenching temperature, although all models show slight difference to the measured peak.

Fig. 12 shows the measured hardness values for the examined steels. The hardness values are presented as average values with standard deviation (St.D.) shown in error bars and numerically below as St.D. A and St.D. B for steels A and B, respectively. The initial hardness of the as-received steels was roughly 200 HV2. As a reference, samples from

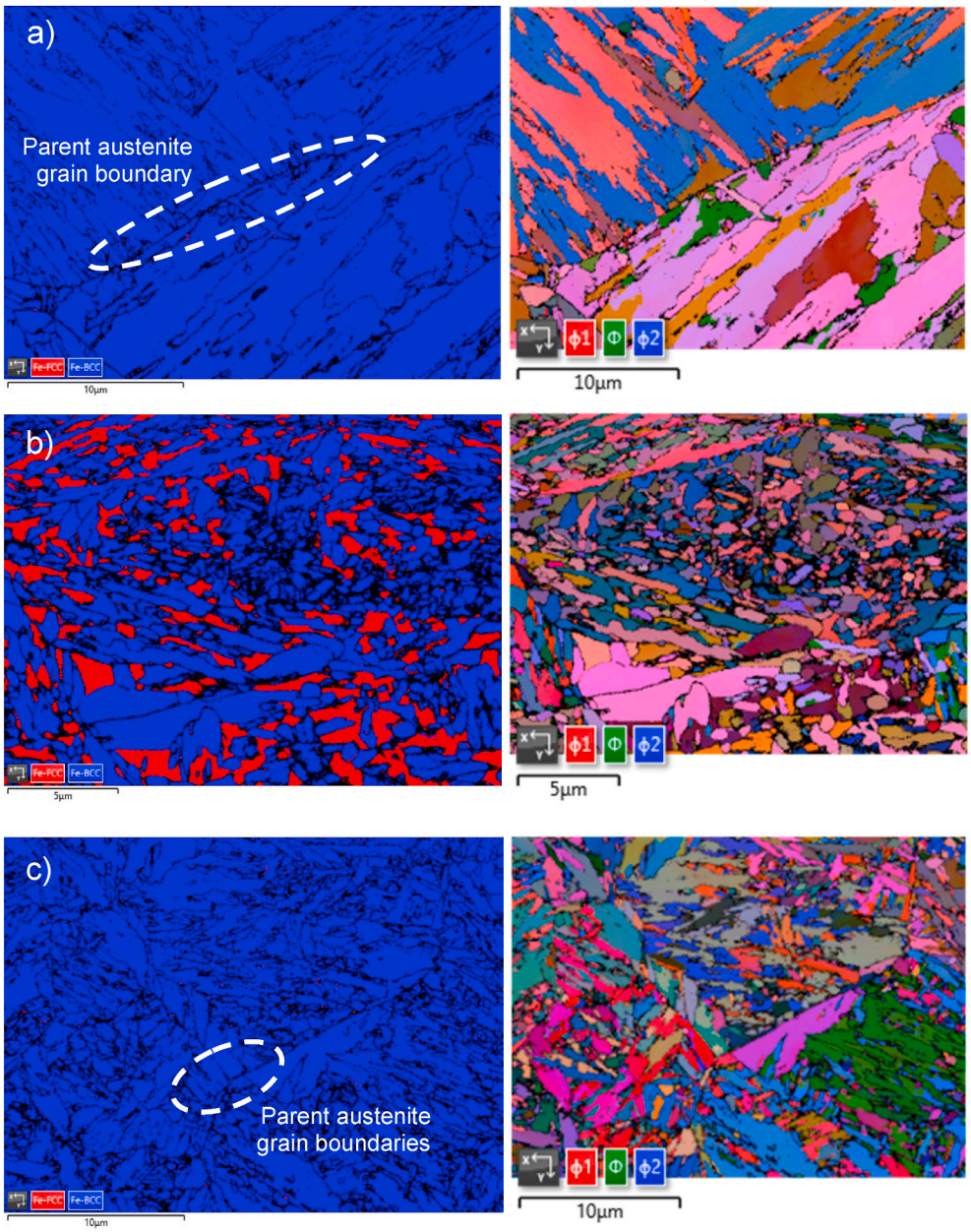

Fig. 9. EBSD micrographs of the phase distribution and Euler angles of the steel B: a) As quenched, and after Q&P with QT of b) 100 °C, and c) 160 °C.

both steels were austenitized and quenched without partitioning step, resulting in hardness values of roughly 575 HV2 and 660 HV2 for steels A and B, respectively. For steel A, the hardness was significantly reduced by the partitioning step after any initial quenching temperature, with measured values varying between 430 HV2 and 500 HV2. A slight decline of hardness can be observed as the quenching temperature is increased towards the highest examined values. For steel B, the Q&P heat treatment has a significant influence on the resulting hardness of the steel. Samples initially quenched at 85 and 100 °C show a clear reduction in hardness, the latter one being the softest at 500 HV2. These results are in accordance with the retained austenite measurements, as these samples contain the highest amounts of retained austenite, hence lowering the hardness of the steel. Interestingly, samples initially quenched at higher temperatures reach similar hardness levels as samples without partitioning, despite moderate retained austenite fraction.

The results of the tensile tests are presented as engineering stress-strain curves in Fig. 13. The stress-strain curves from as-received reference samples were excluded from Fig. 13 for clarity. The 0.2% proof strength ($R_{p0.2}$), ultimate tensile strength (R_m), total elongation (A) and non-proportional elongation at maximum force (A_g) of all samples were measured and summarized in Table 3. It can be clearly seen in Fig. 13 that the quenched and partitioned samples of steel B are not mechanically stable at room temperature: All samples fractured in a brittle manner without detectable plastic deformation. As a result, the ultimate tensile strength cannot be properly compared, as brittle fracture occurs in unpredictable manner between the samples and a small difference in elongation has a significant effect on the measured strength. However, it can be noted that increasing the initial quenching temperature resulted in lower elongation before fracture. Regarding the steel A, Q&P results in high strength level exceeding 1400 MPa with total elongation ranging from 11% to 12.1%. Increase in initial *QT* reduces both 0.2% proof strength as well as ultimate tensile strength while increasing elongation at maximum force as well as total elongation.

Fracture surfaces of the tensile test samples are shown in Fig. 14. A ductile type of fracture can be clearly seen in the reference samples as well as the heat treated samples of steel A (Fig. 14). All samples of the

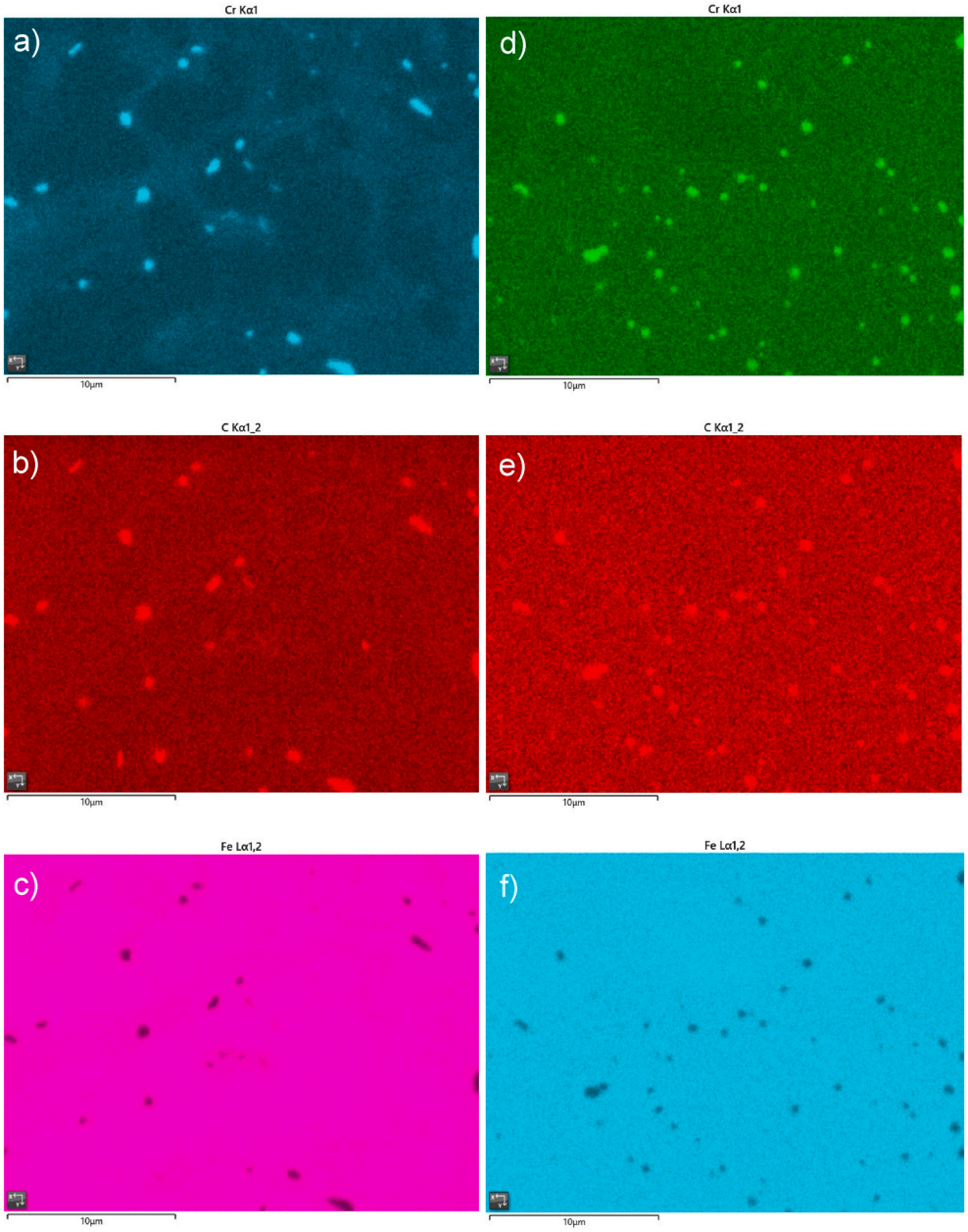

Fig. 10. EDS-spectra of the studied steels: a) for Cr Kα1, b) for C Kα1_2, and c) for Fe Lα1,2 in steel A with QT 170 °C, and d) for Cr Kα1, e) for C Kα1_2, and f) for Fe Lα1,2 in steel B with QT 160 °C.

Table 2
Retained austenite fractions calculated from the XRD data before and after correcting the influence of carbides.

Sample	Data	QT (°C)							
		85	100	115	130	145	160	170	Quenched
Steel A	Unmodified RA(%)	9.6	10.0	9.1	9.5	11.4	12.3	14.4	<1
	Carbide corrected RA(%)	9.4	9.7	8.8	9.3	11.0	11.9	13.8	<1
Steel B	Unmodified RA(%)	16.8	30.5	11.8	14.8	13.2	10.2	5.5	1.7
	Carbide corrected RA(%)	16.2	29.7	11.4	14.5	12.7	7.0	3.3	1.7

steel A showed a ductile type of fracture with some carbides present at the "pits" of the surface. All fractures of the heat treated samples of steel B were brittle type, and the fracture mostly propagated through the grain boundaries. This can be seen in Fig. 14 as fine grain surfaces and visible cracks along the grain boundary.

Additional hardness measurements were performed on the deformed samples. In the steel A the measured hardness values of quenched and partitioned samples ranged from 460 to 490 HV2, similarly to samples before tensile tests. In some samples from steel B, however, the measured hardness values had increased significantly after tensile tests. Before the tensile tests the measured hardness values ranged from circa 500 HV2 (*QT* 100 °C) to 660 HV2 (*QT* 160 °C). In the sample with

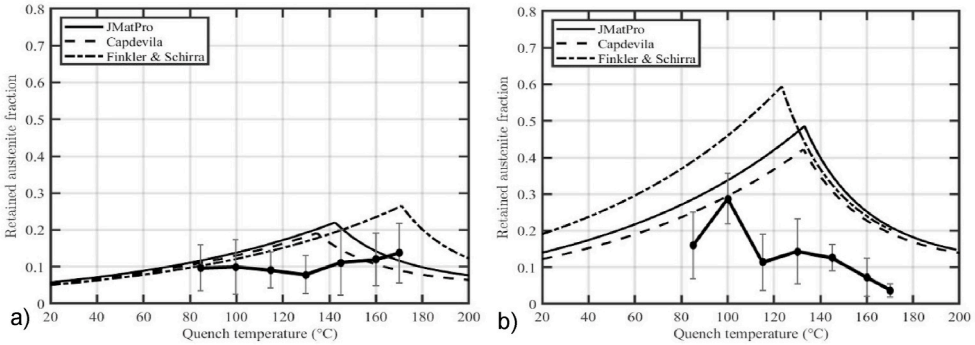

Fig. 11. Measured retained austenite fractions (data points with estimated error bars) and simulated retained austenite fractions (calculation methods shown in legend) of steel A (a) and steel B (b).

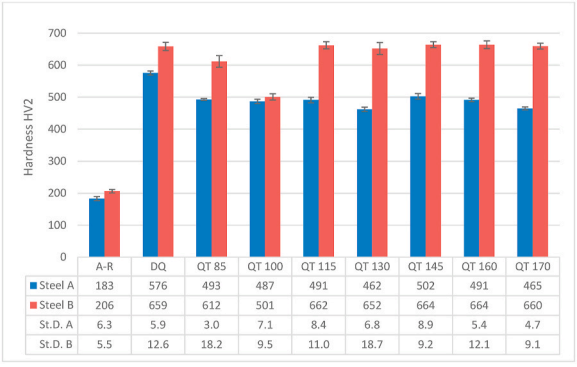

Fig. 12. Hardness test results for samples in as-received condition, after quenching without partition, and after Q&P heat treatments.

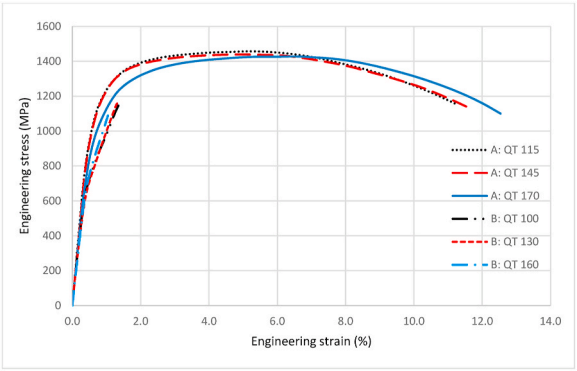

Fig. 13. Tensile test results for steel A and steel B.

Table 3
0.2% proof stress, ultimate tensile strength, total elongation, and non-proportional elongation at maximum force of the tensile test specimen.

Sample	Heat Treatment	Rp0.2 (MPa)	Rm (MPa)	A (%)	Ag (%)
Steel A	Ref	390	550	30.0	16.7
	QT115	1110	1460	11.2	5.3
	QT145	1100	1440	11.4	5.4
	QT170	1010	1430	12.1	6.2
Steel B	Ref	410	650	25.0	12.7
	QT100	850	1150	0.8	0.8
	QT130	830	1160	0.7	0.7
	QT160	910	1090	0.4	0.4

highest initial hardness (*QT* 160 °C) the difference in hardness was negligible after the tensile test, being approximately 670 HV2. In the other samples, however, the measured hardness of the tensile test specimen reached 680 HV2 and 700 HV2 for quenching temperatures of 100 °C and 130 °C, respectively. Especially for the sample *QT* 100 °C the hardness differs greatly from 500 HV2 before tensile test to 680 HV2 after tensile test.

In addition to hardness measurements, XRD-analysis was conducted for the tensile test samples to determine the retained austenite fraction of the uniformly strained area. Measurements from the grip region produced similar results to ones measured earlier in Table 2. In the deformed gauge region, however, the RA-fractions of all samples were lower than within the grip region. The greatest difference was observed in steel B with initial *QT* of 100 °C, where the RA-fraction was reduced from roughly 30%–9.7% after the tensile test. Hence, majority of the retained austenite transformed into martensite during the tensile test.

4. Discussion

4.1. Thermodynamic models

The main aim of this paper was to evaluate different theoretical calculation models for determining for the optimal initial quenching temperature for the Q&P heat treatment of ferritic stainless steels. To the authors' best knowledge, only few models have suitable composition range for modelling stainless steels in this manner. Based on the simulation results in Fig. 11, all the used models result in a similar curve with some deviation in optimal *QT* as well as retained austenite fraction. The similarity of the shapes of the curves is explained by the used transformation kinetics model, the K-M equation, as it has the highest impact on the steepness of the curve. The main drawback of the K-M equation is that the value of multiplier K in equation (1) is considered constant instead of being composition-dependent. Newer models addressing this issue [18–20] indicate that the K-M equation overestimates the retained austenite fraction especially at lower quenching temperatures. None of these models, however, are accurate for stainless steels. Therefore, all theoretical estimations for the optimal *QT* are expected to have a slight offset to the actual values, independent on the M_s temperature model used. This offset, however, could be corrected in the future if a suitable K-M-type equation is developed for stainless steels.

While the shape of the curve in the model is mainly dependent on the K-M-type equation, the optimal *QT* and the estimated retained austenite fraction highly depend on the used M_s temperature model. This can be seen in Fig. 11, especially by comparing simulation results of the steel B: The estimated initial M_s temperature varies from 170 °C produced by equation (3) from Finkler & Schirra [25] to roughly 210 °C produced by equation (2) from Capdevila et al. [26]. Lower initial M_s temperature results in lower optimal *QT* as well as higher estimate for the retained austenite fraction. The other defining factor related to the M_s

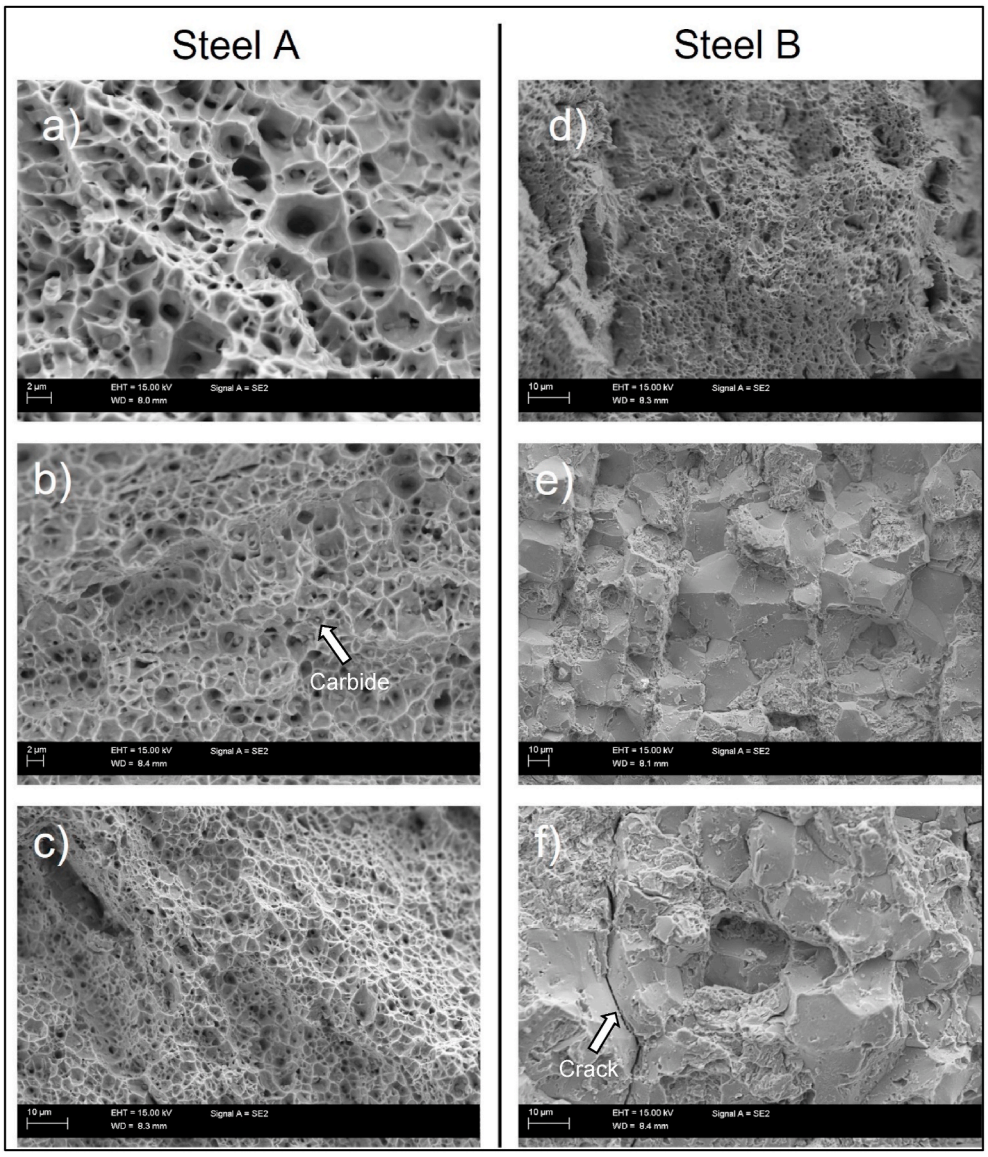

Fig. 14. Fracture surfaces of tensile test samples: Steel A a) reference sample and Q&P-samples b) with QT 145 °C and c) with QT 170 °C, and steel B d) reference sample and Q&P-samples e) with QT 100 °C and f) with QT 160 °C.

temperature calculation is the multiplier of carbon in the model: During the partition step, only carbon is presumed to diffuse, hence making carbon fraction of austenite the only variable within the M_s temperature model. Therefore, the higher the coefficient for carbon is, the less carbon is needed to stabilize austenite at room temperature. As a result, the peak of the curve is moved towards higher initial *QT*, which also leads to higher estimate for retained austenite fraction.

When the simulated models are compared to experimental results, all theoretical models seem to produce higher retained austenite fractions than measurements. This can be explained by two reasons. First of all, the K-M equation assumes slower martensite transformation kinetics than what experimental results [19,20] have shown, leading to slight overestimate for retained austenite fraction. The main deviation between simulated and measured values, however, is very likely caused by carbide formation during the partitioning step. As carbide formation acts as a competing reaction for carbon partitioning to austenite, less carbon is available for stabilizing austenite, and some of the initial austenite will transform into martensite upon final quenching. Based on the micrographs of quenched samples, a small ($< 1\%$) fraction of carbides was presumably still present after the austenitization. This indicates that the austenitization temperature or holding time was not sufficient for full dissolution of carbides. Based on the measured carbide fractions, however, most carbides observed are formed during the partitioning step of the heat treatment. Several studies [8,12,30–33] have reported that chromium-rich M_3C-type carbides may form at the range of the partitioning temperature of 400 °C. Thus, the results of this study are in accordance with those works. Although the measured carbide fractions were low, up to 5% at most, the carbon concentration within a carbide is significantly higher than within the surrounding phases. Therefore, carbide formation effectively limits the maximum gain of retained austenite during the heat treatment. This explains the lower retained austenite fractions measured than what the theoretical CCE-models suggest. Moreover, the reduced carbon enrichment of austenite will move the peak of the optimal *QT* towards lower temperatures.

Despite several reports on M_3C-type carbide precipitation during the Q&P process, few attempts have been made to improve the existing CCE-models to include this competing mechanism. Toji et al. [34] proposed a model for carbon partitioning which includes the effect of cementite formation in high-carbon steels, named as CCEθ-model. In the

CCEθ-model, however, the austenite carbon concentration is considered independent of the initial austenite fraction as well as the bulk carbon content. As a result, the change in initial martensite fraction is only considered to influence the carbide formation, which is not supported by the results of the present study. Changes in fractions of both retained austenite as well as formed carbides suggest that both mechanisms should be considered in the calculation to model the resulting microstructure accurately. This kind of calculation, however, may become rather complex, especially if only theoretical approach is considered. Thus, formulation of a new empirical model may be a more feasible approach for stainless steels. If the fraction of formed carbides can be modelled from empirical measurements, this data could be utilized in the calculation of retained austenite as well.

4.2. Microstructure analysis

The fraction of retained austenite can be measured with both XRD as well as EBSD methods. The XRD method used was direct comparison of integrated intensities of preferred crystallographic orientations. Although the effect of carbide interference within the austenite peaks was calculated, some of the interference on the austenite (220)-peak could not be appropriately assessed. Therefore, the steels are likely to contain slightly higher amount of retained austenite than what was measured.

The retained austenite fraction could also be measured with the EBSD technique. However, the measured fractions of retained austenite were systematically lower than what was measured by the XRD and were excluded from the results. This issue has been addressed in the literature, for example in [9,12,35,36], as some of the datapoints are not accurately indexed. Additionally, most of the EBSD measurements contained relatively large area of non-indexed zero-solution datapoints. Seo et al. [37] reported that these regions may correspond to secondary martensite, as it has a high dislocation density which deteriorates the EBSD pattern quality. However, it is also possible that some of the retained austenite may have transformed into martensite during the sample preparation [36,38].

Although EBSD might not produce accurate data on the retained austenite fraction, it is a valuable tool for assessing the retained austenite distribution. In Fig. 8 the detected retained austenite grains are located at the vicinity of non-indexed areas. These areas correspond to prior grain boundaries or other high angle boundary regions. Wang et al. [39] argued that the retained austenite can be heterogeneously distributed to these regions, as the small austenite grains have more interface area to absorb carbon from the martensite. Considering that the microstructures in Figs. 8 and 9 contain carbides, it is obvious that the carbon distribution within the microstructure is not homogeneous. Furthermore, Hidalgo et al. [40] reported that the carbon concentration in austenite may be inhomogeneous after a partition time of 50 s, whereas homogenized carbon distribution was obtained after 30 min. Therefore, given that the partition time is kept short as in this study, the most stable retained austenite can be presumed to be detected as small grains at high angle boundary regions. However, this does not seem to apply in samples containing a large fraction of retained austenite (Fig. 9 b)). It can be seen in Fig. 9 b) that the retained austenite grains are distributed everywhere within the structure. Furthermore, it should be noted that any retained austenite located in-between the martensite laths can be challenging to locate with EBSD due to poor resolution. Thus, samples in which only a small fraction of retained austenite was detected in EBSD may contain retained austenite in-between the martensite laths as well.

Based on the EDS-spectra shown in Fig. 10, chromium seems to concentrate at the grain boundary regions of the samples. This can be observed as thin brighter areas surrounding darker grains especially in Fig. 10 a) and b), bright particles corresponding to Cr-carbides. While both studied grades had similar carbide contents after high initial *QT* as seen from Fig. 7, their carbide distribution seems to differ slightly. In steel A (Fig. 10 a) and b) and c)), the carbide particles mainly seem to form at the Cr-rich grain boundary region, although some particles are also formed within the martensite. However, despite the grain boundary region having high Cr-content, carbides are not formed universally along the grain boundary, and some grain boundary regions seem to be free of carbides. Conversely, in steel B (Fig. 10 d) and e) and f)) small carbides seem to form alongside the grain boundary, whereas Cr-enrichment at the grain boundary region is not as visible. This suggests that the higher carbon content of steel B could promote carbide formation at the grain boundaries.

4.3. Mechanical properties

The tensile test results show that the mechanical stability of the examined steels varies significantly after Q&P heat treatment. While the steel A showed high ultimate tensile strength levels exceeding 1400 MPa with total elongation of 11–12%, the steel B was unstable at room temperature and all samples fractured in a brittle manner. The poor performance of the steel B can be caused by several reasons. Firstly, the increase of hardness and decrease of retained austenite fractions after tensile test indicate that some of the retained austenite transformed into martensite during the test. Given that there was little plastic deformation, the mechanism causing this was stress-induced austenite-to-martensite transformation. This has also been reported in earlier studies [8,11]. In their work, Huang et al. [11] suggested that due to carbide formation during partitioning, the actual carbon enrichment of austenite would be only a fraction of the theoretical estimate. Hence, the retained austenite becomes very unstable and is easily transformed into brittle martensite by external stress. However, as the fracture surfaces show that the fracture mechanism was mainly intergranular, other mechanisms are more likely to cause the brittle behaviour. Another reason for the brittle fracture in steel B relies on the location of carbides and retained austenite grains. As observed in Fig. 5 c and Fig. 9 b) & c), some of the carbides as well as the retained austenite grains are located at the high-angle grain boundary regions. These regions could act as nucleation sites for cracks which would then propagate along the grain boundaries. This would result in grain boundary cracks visible in Fig. 14. In a study by Rosemann et al. [41] it was shown that carbides may form at the grain boundaries in the steel B after austenitization if the cooling rate is insufficient. For the steel A, however, even low cooling rates of only few K/s did not lead to carbide formation at grain boundaries. This can also be observed in JMatPro®-simulated CCT-curves in Fig. 1, where carbide formation only initiates at cooling rates lower than 1 K/s.

Interestingly, the carbon content of the stainless steels seems to have a significant effect on the ductility after Q&P. For the steel A with a lower carbon content the mechanical properties show combination of high strength with decent ductility after Q&P. Similar results have also been achieved with other stainless steels with low carbon content [31]. With increased carbon content of steel B, however, there has been studies concluding differing results: some with samples breaking in a brittle manner [8,10,11,42] and some achieving good combinations of strength and ductility [8,42,43], depending on the process conditions. Based on these earlier studies, one influencing factor seems to be the partition time: the best mechanical properties were achieved when the partition time was around 30 min. Hidalgo et al. [40] hypothesized that the carbon distribution within the austenite is inhomogeneous during the early stages of partition, whereas longer partition times would homogenize the carbon distribution. Hence, short partition times should be avoided. Uneven carbon distribution could also lead to formation of fresh martensite upon final quenching, as observed in Ref. [33], as some retained austenite grains would be depleted of carbon. This suggests that low initial quenching temperatures should be preferred; otherwise, the microstructure may contain brittle martensite after partition.

In addition to carbide formation at grain boundaries, partition heat treatment at temperatures exceeding 400 °C might expose the examined steels to temper embrittlement. As seen in Table 1, the examined steels

contain phosphorus which may segregate to grain boundaries at a temperature range of 400–600 °C [44]. This is known to cause intergranular fracture type during mechanical testing. Considering that Cr-rich carbides are formed at grain boundaries, depleting them from carbon, it is likely that segregation of phosphorus to the grain boundaries took place during the partition. This could explain the intergranular fractures observed in steel B. Due to the high austenitization temperature of steel B, the parent austenite grain size is also expected to be rather large, which further exposes the steel to temper embrittlement. It has been reported [45,46] that tempering AISI 420-type stainless steel within temperatures of 400–600 °C has resulted in reduction of mechanical properties due to temper embrittlement caused by segregation of Cr and P. To the authors' knowledge, however, this issue has not been addressed in studies related to Q&P of stainless steels. Furthermore, in some studies [8,10,11] the phosphorus content of the steel is not mentioned altogether. This hinders comparison of the effect of temper embrittlement, unless if the steels were completely free of impurities. If the steels would not contain any impurities, those elements would be excluded from the composition and temper embrittlement would be unlikely to occur. This could explain the differences observed in the mechanical properties in different studies of the namely same steel. Without further information about the steel compositions, however, this comparison is entirely hypothetical. In a study by Dieck et al. [42], the phosphorus content of the steel similar to steel B was 0.012%, lower than 0.029% of steel B, and their tensile test results showed brittle fracture with slightly higher elongation compared to this study. Thus, the effect of impurities such as phosphorus should not be ignored. If temper embrittlement cannot be excluded as an influencing factor to the mechanical behaviour, partition temperatures exceeding 400 °C should not be used in stainless steels containing impurities. Since the main requirement for the selection of *PT* is sufficient carbon partition during the heat treatment, lower temperatures could also be used if the partition time is increased correspondingly. Hence, it is possible that the mechanical properties of the examined steels could be enhanced by lowering the partition temperature to slightly above the M_s temperature while increasing the partition time. Further studies on the influence of partition conditions are therefore needed.

5. Conclusions

In this paper, the selection method for obtaining optimal initial quenching temperature during quenching and partitioning of ferritic stainless steels was evaluated. Computer simulations were compared with results from experimental tests for two stainless steels EN 1.4021 (steel A) and EN 1.4034 (steel B). Based on the results, the following conclusions can be made:

- Optimal *QT* for the Q&P heat treatment can be approximated by modelling with limited accuracy only. Experimental results show that the equations used within the model should be chosen according to the steel composition: equations based on composition range similar to the examined steels produce more accurate results. Moreover, careful selection of the modelling parameters can effectively narrow the scale of optimal quenching temperature to a range of roughly 20 °C.
- The retained austenite fractions predicted with current models are systematically overestimated. This is due to formation of chromium-rich carbides, which acts as a competing mechanism to carbon partition during the heat treatment. This offset could be corrected in the future by creating a model considering both mechanisms for carbon during partition.
- Microstructure analysis revealed that the formation of carbides is correlated to the initial quenching temperature with higher *QT* resulting in increased carbide formation. In steel B with higher carbon content some carbides form at parent austenite grain boundaries.
- Q&P processing can be applied to grade EN 1.4021 stainless steel, resulting in high ultimate tensile strength levels exceeding 1400 MPa with total elongation of 11–12%. For the grade EN 1.4034 Q&P processing did not produce stable mechanical properties at room temperature, and all samples fractured in a brittle manner. Variation of *QT* and retained austenite content had only slight influence on the mechanical properties.
- Fracture surfaces of EN 1.4034 showed intergranular fracture type. Potential cause for the brittle fracture is temper embrittlement due to segregation of phosphorus at partition temperature of 400 °C. To avoid temper embrittlement, lower partition temperatures should be used. More research on the influence of partition conditions is needed in the future.

Funding

This work was supported by the Technology Industries of Finland Centennial Foundation Steel and Metal Producers' Fund [2018/2020].

Data availability statement

The raw/processed data required to reproduce these findings cannot be shared at this time as the data also forms part of an ongoing study. The data related to modelling can be made available upon reasonable request to the corresponding author.

CRediT authorship contribution statement

Lassi Raami: Conceptualization, Methodology, Investigation, Data curation, Software, Writing – original draft. **Pasi Peura:** Validation, Supervision, Resources, Funding acquisition, Writing – review & editing.

Declaration of competing interest

The authors declare that they have no known competing financial interests or personal relationships that could have appeared to influence the work reported in this paper.

Acknowledgements

This work made use of Tampere Microscopy Center facilities at Tampere University.

References

[1] J.G. Speer, E. De Moor, K.O. Findley, D.K. Matlock, B.C. De Cooman, D. V. Edmonds, Analysis of microstructure evolution in quenching and partitioning automotive sheet steel, in: Metallurgical and Materials Transactions A: Physical Metallurgy and Materials Science, 2011, pp. 3591–3601.
[2] D.K. Matlock, J.G. Speer, Third generation of AHSS: microstructure design concepts, in: Microstructure and Texture in Steels, Springer London, 2009, pp. 185–205.
[3] J. Speer, D.K. Matlock, B.C. De Cooman, J.G. Schroth, Carbon partitioning into austenite after martensite transformation, Acta Mater. 51 (9) (2003 May 23) 2611–2622.
[4] A.J. Clarke, J.G. Speer, M.K. Miller, R.E. Hackenberg, D.V. Edmonds, D.K. Matlock, et al., Carbon partitioning to austenite from martensite or bainite during the quench and partition (Q&P) process: a critical assessment, Acta Mater. 56 (1) (2008) 16–22.
[5] E. De Moor, J.G. Speer, D.K. Matlock, J.H. Kwak, S.B. Lee, Quenching and partitioning of CMnSi steels containing elevated manganese levels, Steel Res. Int. 83 (4) (2012) 322–327. https://doi.org/10.1002/srin.201100318.
[6] D.T. Pierce, D.R. Coughlin, D.L. Williamson, K.D. Clarke, A.J. Clarke, J.G. Speer, et al., Characterization of transition carbides in quench and partitioned steel microstructures by Mössbauer spectroscopy and complementary techniques, Acta Mater. 90 (2015 May 15) 417–430.
[7] M. Wendler, C. Ullrich, M. Hauser, L. Krüger, O. Volkova, A. Weiß, et al., Quenching and partitioning (Q& P) processing of fully austenitic stainless steels, Acta Mater. 133 (2017 Jul 1) 346–355, https://doi.org/10.1016/j.actamat.2017.05.049. https://www.sciencedirect.com/science/article/pii/S1359645417304366.

[8] L. Yuan, D. Ponge, J. Wittig, P. Choi, J.A. Jiménez, D. Raabe, Nanoscale austenite reversion through partitioning, segregation and kinetic freezing: example of a ductile 2 GPa Fe–Cr–C steel, Acta Mater. 60 (6–7) (2012 Apr 1) 2790–2804, https://doi.org/10.1016/j.actamat.2012.01.045. https://www.sciencedirect.com/science/article/pii/S1359645412000833#!.
[9] J. Mola, B.C. De Cooman, Quenching and partitioning (Q&P) processing of martensitic stainless steels, Metall. Mater. Trans. A Phys. Metall. Mater. Sci. 44 (2) (2013) 946–967. https://doi.org/10.1007/s11661-012-1420-1.
[10] Q. Huang, O. Volkova, B.C. De Cooman, H. Biermann, J. Mola, Influence of Si addition on the carbon partitioning process in martensitic-austenitic stainless steels, IOP Conf. Ser. Mater. Sci. Eng. 373 (2018), 012001. https://doi.org/10.1088/1757-899X/373/1/012001.
[11] Q. Huang, C. Schröder, H. Biermann, O. Volkova, J. Mola, Influence of martensite fraction on tensile properties of quenched and partitioned (Q&P) martensitic stainless steels, Steel Res. Int. 87 (8) (2016) 1082–1094.
[12] S.Y. Lu, K.F. Yao, Y.B. Chen, M.H. Wang, N. Chen, X.Y. Ge, Effect of quenching and partitioning on the microstructure evolution and electrochemical properties of a martensitic stainless steel, Corrosion Sci. 103 (2016 Feb 1) 95–104.
[13] J.G. Speer, D.V. Edmonds, F.C. Rizzo, D.K. Matlock, Partitioning of carbon from supersaturated plates of ferrite, with application to steel processing and fundamentals of the bainite transformation, Curr. Opin. Solid State Mater. Sci. 8 (3–4) (2004) 219–237.
[14] D.V. Edmonds, K. He, F.C. Rizzo, B.C. De Cooman, D.K. Matlock, J.G. Speer, Quenching and partitioning martensite-A novel steel heat treatment, Mater. Sci. Eng. A 438–440 (2006) 25–34 (SPEC. ISS.).
[15] M. Hillert, J. Ågren, On the definitions of paraequilibrium and orthoequilibrium, Scripta Mater. 50 (5) (2004 Mar) 697–699.
[16] M. Hillert, J. Ågren, Reply to comments on "On the definition of paraequilibrium and orthoequilibrium, in: Scripta Materialia, 52, Elsevier Ltd, 2005, pp. 87–88.
[17] D.P. Koistinen, R.E. Marburger, A General Equation Prescribing the Extent of the Austenite-Martensite Transformation in Pure Iron-Carbon Alloys and Plain Carbon Steels, 7, Acta Metallurgica. Pergamon, 1959, pp. 59–60.
[18] S.M.C. Van Bohemen, J. Sietsma, Martensite formation in partially and fully austenitic plain carbon steels, Metall. Mater. Trans. 40 (5) (2009 May) 1059–1068, https://doi.org/10.1007/s11661-009-9796-2.
[19] S.J. Lee, C.J. Van Tyne, A kinetics model for martensite transformation in plain carbon and low-alloyed steels, Metall. Mater. Trans. A Phys. Metall. Mater. Sci. 43 (2) (2012 Feb 8) 422–427.
[20] E.J. Seo, L. Cho, B.C. De Cooman, Modified methodology for the quench temperature selection in quenching and partitioning (Q&P) processing of steels, Metall. Mater. Trans. A Phys. Metall. Mater. Sci. 48 (8) (2016 Aug 7) 3797–3802. https://doi.org/10.1007/s11661-016-3579-3.
[21] K.W. Andrews, Empirical formulas for the calculation of some transformation temperatures, J. Iron Steel Inst. 203 (7) (1965) 721–727.
[22] H.K.D.H. Bhadeshia, Thermodynamic extrapolation and martensite-start temperature of substitutionally alloyed steels, Met. Sci. 15 (4) (1981 Apr 1) 178–180.
[23] J. Wang, PJ van der Wolk, S van der Zwaag, Determination of martensite start temperature in engineering steels Part I. Empirical relations describing the effect of steel chemistry, Mater. Trans., JIM 41 (7) (2000) 761–768. https://doi.org/10.2320/matertrans1989.41.761.
[24] C. Capdevila, F.G. Caballero, C. García De Andrés, Determination of Ms temperature in steels: a Bayesian neural network model, ISIJ Int. 42 (8) (2002) 894–902. https://doi.org/10.2355/isijinternational.42.894.
[25] H. Finkler, M. Schirra, Transformation behaviour of the high temperature martensitic steels with 8 - 14% chromium, Steel Res. 67 (8) (1996 Aug) 328–342. https://doi.org/10.1002/srin.199605498.
[26] C. Capdevila, F.G. Caballero, C. García de Andrés, Analysis of effect of alloying elements on martensite start temperature of steels, Mater. Sci. Technol. 19 (5) (2003 May 1) 581–586.
[27] A. Hultgren, Isothermal transformation of austenite, Trans. Am. Soc. Mater. 39 (1947) 915–989.
[28] C.G. De Andrés, G. Caruana, L.F. Alvarez, Control of M23C6 carbides in 0.45C-13Cr martensitic stainless steel by means of three representative heat treatment parameters, Mater. Sci. Eng. A 241 (1–2) (1998 Jan 1) 211–215.
[29] ASTM, E975 - 13, Standard Practice for X-Ray Determination of Retained Austenite in Steel with Near Random Crystallographic Orientation, ASTM International, 2013, pp. 1–7. Available from: https://www.astm.org/Standards/E975.
[30] Q. Huang, M. Yao, I. Timokhina, C. Schimpf, H. Biermann, O. Volkova, et al., Tempering reactions and elemental redistribution during tempering of martensitic stainless steels, Metall. Mater. Trans. A Phys. Metall. Mater. Sci. 50 (8) (2019 Aug 15) 3663–3673. https://doi.org/10.1007/s11661-019-05272-3.
[31] T. Tsuchiyama, J. Tobata, T. Tao, N. Nakada, S. Takaki, Quenching and partitioning treatment of a low-carbon martensitic stainless steel, Mater. Sci. Eng. A 532 (2012 Jan 15) 585–592. https://doi.org/10.1016/j.msea.2011.10.125.
[32] J. Tobata, K.L. Ngo-Huynh, N. Nakada, T. Tsuchiyama, S. Takaki, Role of silicon in quenching and partitioning treatment of lowcarbon martensitic stainless steel, ISIJ Int. 52 (7) (2012) 1377–1382.
[33] S. Dieck, P. Rosemann, A. Kromm, T. Halle, Reversed austenite for enhancing ductility of martensitic stainless steel, IOP Conf. Ser. Mater. Sci. Eng. 181 (2017 Mar), 012034. https://doi.org/10.1088/1757-899X/181/1/012034.
[34] Y. Toji, G. Miyamoto, D. Raabe, Carbon partitioning during quenching and partitioning heat treatment accompanied by carbide precipitation, Acta Mater. 86 (2015) 137–147.
[35] C. Parish, T. Watkins, O. Rios, G. Mackiewicz-Ludtka, G. Ludtka, O. Cavin, Characterization of retained austenite and carbides in stainless steel by combined EBSD, EDS, and XRD, Microsc. Microanal. 17 (S2) (2011 Jul) 410–411. https://doi.org/10.1017/S1431927611002923.
[36] S. Uusikallio, A. Kisko, T.T. Nyo, D.A. Porter, J. Kömi, M. Jaskari, Sample preparation challenges with highly metastable ferritic-austenitic stainless steels, Prakt. Metallogr. Metallogr. 56 (6) (2019) 373–392.
[37] E.J. Seo, L. Cho, Y. Estrin, B.C. De Cooman, Microstructure-mechanical properties relationships for quenching and partitioning (Q&P) processed steel, Acta Mater. 113 (2016) 124–139.
[38] K.R. Elstad, B.S. Andresen, M. Karlsen, I. Westermann, J. Hjelen, The effect of sample preparation on quantification of retained austenite in supermartensitic stainless steel studied by EBSD and XRD, in: Twenty-sixth International Ocean and Polar Engineering Conference, ISOPE (2016 Jun 26), 2016 Jun 26. Available from: https://www.researchgate.net/publication/306018130_The_Effect_of_Sample_Preparation_on_Quantification_of_Retained_Austenite_in_Supermartensitic_Stainless_Steel_Studied_by_EBSD_and_XRD.
[39] C.Y. Wang, J. Shi, W.Q. Cao, H. Dong, Characterization of microstructure obtained by quenching and partitioning process in low alloy martensitic steel, Mater. Sci. Eng. A 527 (15) (2010 Jun 15) 3442–3449.
[40] J. Hidalgo, K.O. Findley, M.J. Santofimia, Thermal and mechanical stability of retained austenite surrounded by martensite with different degrees of tempering, Mater. Sci. Eng. A 690 (2017 Apr 6) 337–347.
[41] P. Rosemann, C. Müller, N. Kauss, T. Halle, Einfluss der Abkühlgeschwindigkeit auf die Neigung zur Chromverarmung martensitischer nichtrostender Stähle, Madgeburg, 2017 [cited 2021 Feb 3]. Available from: https://www.researchgate.net/publication/322132093_Einfluss_der_Abkuhlgeschwindigkeit_auf_die_Neigung_zur_Chromverarmung_martensitischer_nichtrostender_Stahle.
[42] S. Dieck, M. Ecke, P. Rosemann, T. Halle, Verbesserung der Eigenschaften vom martensitischen, nichtrostenden Stahl X46Cr13 durch Q& P-Wärmebehandlung, 2017 [cited 2020 Jul 21]; Available from: https://www.researchgate.net/publication/322132179_Verbesserung_der_Eigenschaften_vom_martensitischen_nichtrostenden_Stahl_X46Cr13_durch_QP-Warmebehandlung.
[43] S. Dieck, M. Ecke, P. Rosemann, S. Fritsch, M. Franz-Xaver Wagner, T. Halle, et al., Strength differential effect in martensitic stainless steel under quenching and partitioning heat treatment condition, in: H. Altenbach, M. Brünig, Z. Kowalewski (eds), Plasticity, Damage and Fracture in Advanced Materials, Adv. Struct. Mater. 121 (2020) 35–42. Springer, Cham, https://doi.org/10.1007/978-3-030-34851-9_3.
[44] G.V. Prabhu Gaunkar, A.M. Huntz, P. Lacombe, Role of carbon in embrittlement phenomena of tempered martensitic 12Cr-0.15%C steel, Met. Sci. 14 (7) (1980) 241–252. https://doi.org/10.1179/030634580790426427.
[45] K. Chandra, V. Kain, N. Srinivasan, I. Samajdar, A.K. Balasubrahmanian, Temper embrittlement and corrosion behaviour of martensitic stainless steel 420, Adv. Mater. Res. 794 (2013 Sep) 757–765. https://doi.org/10.4028/www.scientific.net/amr.794.757.
[46] A.N. Isfahany, H. Saghafian, G. Borhani, The effect of heat treatment on mechanical properties and corrosion behavior of AISI420 martensitic stainless steel, J. Alloys Compd. 509 (9) (2011 Mar 3) 3931–3936.